Title

Diagnostic Accuracy of Macular Thickness Map and Texture En Face Images for Detecting Glaucoma in Eyes With Axial High Myopia

Authors

Bowd, Christopher

Belghith, Akram

Rezapour, Jasmin

et al.

Publication Date

2022-10-01

DOI

10.1016/j.ajo.2022.04.019

Peer reviewed

HHS Public Access

Author manuscript

Am J Ophthalmol. Author manuscript; available in PMC 2024 March 27.

Published in final edited form as:

Am J Ophthalmol. 2022 October ; 242: 26–35. doi:10.1016/j.ajo.2022.04.019.

Diagnostic accuracy of macular thickness map and texture en-face images for detecting glaucoma in eyes with axial high myopia.

Christopher Bowd, PhD[1], **Akram Belghith, PhD**[1], **Jasmin Rezapour, MD**[1,2], **Mark Christopher, PhD**[1], **Leslie Hyman, PhD**[6], **Jost B. Jonas, MD**[3,4,5], **Robert N. Weinreb, MD**[1], **Linda M. Zangwill, PhD**[1]

[1]Hamilton Glaucoma Center, Shiley Eye Institute, Viterbi Family Department of Ophthalmology, UC San Diego, La Jolla, CA, United States

[2]Department of Ophthalmology, University Medical Center of the Johannes Gutenberg University Mainz, Germany

[3]Department of Ophthalmology, Medical Faculty Mannheim, Heidelberg University, Mannheim, Germany

[4]Privatpraxis Prof Jonas und Dr Panda-Jonas, Heidelberg, Germany

[5]Institute of Molecular and Clinical Ophthalmology Basel, Switzerland

[6]Vision Research Center, Wills Eye Hospital, Philadelphia, PA, United States

Abstract

Purpose: To evaluate the diagnostic accuracy of a novel optical coherence tomography (OCT) texture-based *en-face* image analysis, called SALSA-Texture, that requires segmentation of only one retinal layer for glaucoma detection in eyes with axial high myopia, and to compare to standard macular ganglion cell-inner plexiform layer (GCIPL) thickness, macular retinal nerve fiber layer (mRNFL) thickness, and ganglion cell complex (GCC) thickness maps.

Design: Comparison of diagnostic approaches.

Methods: Cross-sectional data were collected from 92 primary open-angle glaucoma (POAG) eyes and 44 healthy eyes with axial high myopia (axial length > 26 mm). OCT texture *en-face* images, developed using SALSA-Texture to model the spatial arrangement patterns of the pixel intensities in a region, were generated from 70-μm slabs just below the vitreal border of the inner limiting membrane (ILM). Areas under the receiver operating curves (AUROC) and areas under the precision recall curves (AUPRC) adjusted for both eyes, AL, age, disc area and image quality were used to compare different approaches.

Results: The best parameter-adjusted AUROCs (95% CI) for differentiating between healthy and glaucoma high myopic eyes were 0.92 (0.88, 0.94) for texture *en-face* images, 0.88 (0.86, 0.91) for macular RNFL thickness, 0.87 (0.83, 0.89) for macula GCIPL thickness, and 0.87 (0.84, 0.89)

*Corresponding author: Linda M. Zangwill, 9500 Gilman Drive, La Jolla, CA 92093-0946, Shiley Eye Institute/Hamilton Glaucoma Center, Viterbi Family Department of Ophthalmology, University of California, San Diego, lzangwill@health.ucsd.edu.

for GCC thickness. A subset analysis of highly advanced myopic eyes (axial length ≥ 27 mm, 38 glaucomatous eyes and 22 healthy eyes) showed the best AUROC was 0.92 (0.89, 0.94) for texture *en-face* images compared to 0.86 (0.84 , 0.88) for macular GCIPL, 0.86 (0.84, 0.88) GCC and 0.84 (0.81, 0.87) for RNFL thickness ($p \leq 0.02$ compared to texture for all comparisons).

Conclusion: The current results suggest that our novel *en-face* texture-based analysis method can improve on most investigated macular tissue thickness measurements for discriminating between highly myopic glaucomatous and highly myopic healthy eyes. While further investigation is needed, texture *en-face* images show promise for improving the detection of glaucoma in eyes with high myopia where traditional retinal layer segmentation often is challenging.

Graphical Abstract

The diagnostic accuracy of a novel OCT texture-based macular *en-face* image analysis method (called SALSA-Texture) that requires segmentation of only one retinal layer is compared to standard macular ganglion cell-inner plexiform layer (GCIPL) thickness, macular retinal nerve fiber layer (mRNFL) thickness, and ganglion cell complex (GCC) thickness maps for the detection of glaucoma in axial high myopia eyes (axial length > 26 mm). SALSA-Texture shows improved classification when compared to most standard OCT thickness measurements in the current sample.

Myopia is projected to affect 50% of the world's population by 2050[1] with strong epidemiologic evidence linking myopia with glaucoma.[2] Individuals with myopia are 2.5x more likely to have glaucoma than non-myopic individuals[3] while high myopes are 5–6x more likely than non-myopes to have glaucomatous optic neuropathy.[4]

Optical imaging of the optic nerve head (ONH) and the circumpapillary regions pose significant challenges for glaucoma detection in myopic eyes due to ONH tilt, increased ovality of the optic nerve head, and large areas of peripapillary atrophy (PPA), particularly in highly myopic eyes where these anatomical changes can be extreme. Furthermore, circumpapillary retinal nerve fiber layer (cpRNFL) thickness peaks shift temporally in myopic eyes which leads to reduced ability to accurately detect cpRNFL thinning compared to reference normative databases.[5–8] In addition, increased axial length significantly reduces measured cpRNFL thickness and to a lesser degree ganglion cell-inner plexiform layer (GCIPL) thickness in healthy myopic eyes, thus increasing possible confusion between myopia and glaucoma in eyes with both conditions.[9]

Recent evidence suggests that wide-field thickness maps, including optic disc, cpRNFL and macular GCIPL regions, obtained using swept-source OCT (Topcon DRI-OCT) can detect glaucomatous structural defects in myopic eyes better than normative database assessment of parapapillary regions using conventional spectral-domain OCT (Zeiss Cirrus HD OCT).[10] It also has been shown that wide-field DRI-OCT reflectance intensity images can resolve glaucomatous damage detectable using high-resolution adaptive optics- scanning light ophthalmoscopy (AO-SLO) while OCT RNFL thickness maps generated from the same OCTA data cannot.[11] Both of these results, coupled with results indicating that Cirrus HD OCT GCIPL segmentation errors are often observed in myopic eyes[12], suggest that

OCT-based *en-face* images that require minimal retinal layer segmentation may improve detection of glaucoma related defects in eyes both with and without myopia.

Because of the difficulty in detecting glaucomatous defects in myopic eyes and because of the reported superiority of *en-face* image evaluation for successfully detecting glaucoma-related structural defects, the current study evaluated the diagnostic accuracy of a novel, texture-based *en-face* image assessment of macular GCIPL thickness, macular retinal nerve fiber layer (mRNFL) thickness and GCC (ganglion cell complex; GCIPL + mRNFL) thickness measured by spectral-domain OCT for glaucoma detection in axial high myopic eyes.

Methods

Participants included in this cross-sectional observational study were recruited from the Diagnostic Innovations in Glaucoma Study (DIGS). Details of the DIGS protocol have been described previously.[13] The University of California San Diego (UCSD) Institutional Review Board and Human Subjects Committee approved all protocols, and methods adhered to the Declaration of Helsinki. This study was registered at http://clinicaltrials.gov (no. NCT00221923) on September 14, 2005. All study images were obtained from July 2017 to October 2020.

Participants

All participants underwent an extensive ophthalmologic examination, including assessment of best-corrected visual acuity, slit-lamp biomicroscopy, intraocular pressure (IOP) measurement with Goldmann applanation tonometry, gonioscopy, central corneal thickness (CCT) measured with ultrasound pachymetry (DGH Technology, Inc, Exton, Pennsylvania, USA), dilated fundus examination, simultaneous stereophotography of the optic disc, visual field testing by standard automated perimetry (Humphrey Field Analyzer; 24– 2 Swedish interactive threshold algorithm standard; Carl Zeiss Meditec, Jena, Germany), and Spectralis OCT (version 6.10; Heidelberg Engineering Inc, Heidelberg, Germany).

Overall inclusion criteria were age ≥ 18 years, open anterior chamber angles on gonioscopy, and a best-corrected visual acuity of 20/40 or better at study entry. Exclusion criteria were history of intraocular surgery (except for uncomplicated cataract or uncomplicated glaucoma surgery), coexisting retinal pathology, non-glaucomatous optic neuropathy, uveitis, or ocular trauma; diagnosis of Parkinsońs disease, Alzheimeŕs disease or other forms of dementia, or history of stroke; diabetic or hypertensive retinopathy; unreliable visual fields; and poor-quality spectral-domain OCT scans.

All visual fields were evaluated by the University of California, San Diego (UCSD) Visual Field Assessment Center (VisFACT) personnel based on a standardized protocol.[13] Visual fields with more than 33% fixation losses or more than 33% false-positive errors were automatically excluded. Visual fields exhibiting a learning effect (i.e., initial tests with reduced sensitivity followed by consistent improvement in a series of tests) also were excluded. Visual fields were further reviewed for lid and rim artifacts, fatigue effects, evidence that the visual field results were due to a disease other than glaucoma (e.g.,

homonymous hemianopia), and inattention. Test results indicating these characteristics were excluded.

Primary open angle glaucoma was defined based on the DIGS conventional standard of glaucomatous visual field loss and locally corresponding optic disc/parapapillary damage.[13] Stereo photograph-based glaucomatous damage was defined as focal or diffuse narrowing of the neuroretinal rim, and/or cpRNFL defects characteristic of glaucoma based on a masked assessment by two trained observers. Two experts (JR and CB) graded photographs after high myopia optic disc grading training with a senior consultant (JBJ) with expertise in myopia and glaucoma. Stereo photograph-based optic disc damage was defined by consensus between both graders. In case of disagreement, diagnosis was defined by adjudication by the senior consultant. A total of 12/136 (8.8%) clinically ambiguous eyes were referred for consensus/adjudication.

Healthy individuals contributing OCT images had IOP < 21 mm Hg with no history of elevated IOP; normal-appearing optic disc and intact neuroretinal rim and cpRNFL; and a minimum of 2 reliable and normal visual fields defined as a pattern standard deviation (PSD) within 95% confidence limits and a glaucoma hemifield test (GHT) result within normal limits in both eyes. Patient and eye characteristics by diagnosis are shown in Table 1.

All study eyes had high axial myopia defined as axial length > 26.0 mm as described below.

Optical coherence tomography

Spectralis OCT (version 6.10; Heidelberg Engineering Inc, Heidelberg, Germany) was used for image acquisition. This instrument uses an 870-nm central wavelength at an 85-kHz A-scan rate. The custom wide scan type used was an OCT cube of 30° × 25° (8.7 × 7.3 mm) centered on the fovea formed by 121 horizontal B-scans (Figure 1a). The interval between the B-scans was 60 μm and the lateral resolution was 5.64 μm/pixel; the axial resolution was 3.87 μm/pixel, and the frame rate was 10 per B-scan. Quality review of Spectralis images required a signal strength > 15 dB what was deemed acceptable quality for use based on subjective assessment according to the UCSD Imaging Data Evaluation and Assessment Reading Center.

Retinal layer segmentation

Raw three-dimensional SD-OCT images were exported to a numerical computing language (MATLAB; MathWorks, Natick, MA). The San Diego Automated Layer Segmentation Algorithm (SALSA)-deep was used to automatically segment the ILM, mRNFL and IPL layers. In brief, we applied the BCDU-Net approach[14], utilizing Keras with TensorFlow as the backend. The network was trained from scratch using 56000 b-scans obtained from an independent data set as the ground truth. The ADAM optimization technique with a learning rate of 2 × 10−4 and binary cross-entropy loss was used. We stopped the training of the network when the validation loss remained the same in 5 consecutive epochs. The deep layer retinal layer segmentation was manually reviewed for accuracy by investigator AB. GCIPL, mRNFL and GCC (GCIPL + mRNFL) thickness measurements were obtained from each retinal layer within inner (1 mm to 3 mm fovea-centred circular band) and outer (3 mm to 6 mm fovea-centred circular band) measurement rings similar to the instrument defined rings.

Ninety-degree superior, temporal, inferior, and nasal measurements also were obtained from each measurement ring.

High axial myopia defined

In the current study myopia was defined based on axial length rather than refractive error because axial length is most associated with myopia-related changes to the posterior fundus.[15] We defined high axial myopia as eyes with axial length > 26.0 mm as we have done previously.[16]

Texture *en-face* images

Texture can be characterized as a visual pattern that reflects spatial arrangement of pixel intensities of an image. Texture analysis captures the granularity and repetitive patterns of object surfaces. In the case of OCT images, each retinal layer has a unique texture that can be visually distinguished. In this study, we propose a new texture transformation called the San Diego Automated Layer Segmentation Algorithm-Texture (SALSA-Texture) which is robust to the intensity variation of local region caused by illumination. For each pixel ***i*** in a B-scan, we create a 9×9 neighboring system by selecting the 9×9 area surrounding the pixel then we apply a local Gaussian filter to reduce the noise. To increase the robustness to local contrast differences, we use Homogeneous-bin (H-bin) normalization[17] to normalize the NDG descriptor. We then calculate the average difference between the pixel and each other pixel in the 9×9 neighboring system (Figure 1). Finally, texture *en-face* images were generated from 70-μm slabs following the inner limiting membrane (ILM). The slab thickness of 70 μm was calculated as the 25th percentile of the GCC layer thickness. Hence, it is small enough to be affected by local changes but large enough to increase signal-to-noise by averaging over a greater number of pixels. We calculated the projection images (en-face texture image) by averaging the normalized intensity of a fixed axial portion of each A-line of the B-scan, thus creating an image of a “slab” with fixed thickness (70um) below the ILM layer. Outputs used for analyses were average *en-face* image intensities.

Statistical Analyses

Descriptive statistics included mean and 95% confidence intervals (CI). Student’s t-tests or Mann-Whitney tests were used to evaluate demographic and clinical differences between glaucoma patients and healthy individuals.

Both areas under the receiver operating curve (AUROC) and areas under the precision-recall curves (AUPRC) were used to assess the ability of instrument-defined tissue thickness measurements and custom *en-face* texture analysis to discriminate between eyes with glaucoma and healthy eyes and to control for training/test set size imbalance. As measurements from both eyes of the same subject are likely to be correlated, the cluster of data for the study subject were considered as the unit of resampling and bias corrected standard errors (SEs) were calculated. AUROCs and AUPRCs were adjusted for inclusion of both eyes and for age, image quality, axial length, as possible confounders and compared statistically using the Wald test based on the bootstrap covariance.

We also performed several subset analyses using the methods described above. First, because evidence suggests that as axial length greater than 26 mm the number of tissue layer segmentation failures also increase[12] we performed a subset analysis comparing our *en- face* texture analysis to GCIPL, mRNFL and GCC thickness in eyes with AL ≥ 27 mm (this cut-off has been used in other studies to define a subset of high axial myopia[18,19]).

Other subset analyses were performed because age and race were imbalanced between healthy and glaucoma participants. Because healthy individuals were younger than glaucoma patients, we performed a subset analysis comparing measurements in age-matched healthy and glaucoma eyes (healthy eyes [n=21, mean age = 55.9 years; 95% CI = 53.9, 57.8; and glaucoma eyes, n = 48, mean age = 58.2 years, 95% CI = 55.4, 59.6] p = 0.11). Because the percentage of study participants of European descent was lower in the healthy compared to the glaucoma group, we also performed a subset analysis comparing measurements in race-matched healthy and glaucoma eyes (healthy eyes [n=44, European descent, 33%] and glaucoma eye [n = 62, European descent, 37%] p=023).

Statistical analyses were performed using Stata 14.2 (StataCorp LLC, College Station, TX). P values less than 0.05 were considered statistically significant.

Results

One hundred thirty-six glaucoma eyes of 79 patients were included with 92 eyes (55 patients) in the high myopia glaucomatous group and 44 eyes (24 patients) in the high myopia healthy group (Table 1). Mean (95% CI) age (years) in the healthy group was significantly younger (48.9 [46.7, 54.3]) compared to the glaucoma group (65.9 [63.2, 68.5]) ($p < 0.001$). The glaucoma group had worse visual field mean deviation (MD) ($P < 0.001$) than the healthy group. The proportion of individuals of European descent was lower in the healthy group (33%) compared to the glaucoma group (58%) ($p = 0.03$). There was no significant difference in AL ($p = 0.41$) and IOP ($p = 0.52$) between groups. Mean spherical equivalent was significantly lower in healthy group (−7.35 [−7.67, −6.98] dpt) compared to glaucoma group (−4.76 [−5.21, −4.31] dpt) likely due in part to the higher prevalence of cataract surgery in the glaucoma group (42.4%) compared to the healthy group (13.7%).

Table 2 shows AUROCs for classifying glaucoma and healthy eyes within global inner and outer measurement rings for texture based, GCIPL, mRNFL and GCC measurements. Results indicate that diagnostic accuracy for texture-based analysis was highest in the outer measurement ring (0.91 [0.88, 0.93]), accuracy for GCIPL thickness was highest in the inner measurement ring (0.84 [0.82, 0.87]), accuracy for mRNFL thickness was highest in the outer measurement ring (0.88 [0.86, 0.91]), and accuracy for GCC thickness was highest in the inner measurement ring (0.86 [0.84, 0.87]) (Figure 2). The best texture-based AUROC was significantly higher than the best GCC thickness AUROC.

Table 3 shows AUROCs for sectoral (temporal, superior, nasal, inferior) inner and outer measurement rings for all measurements described above. Results indicate that the diagnostic accuracy (AUROC [95% CI]) for classifying eyes by *en-face* texture analysis was highest for outer nasal ring thickness (0.92 [0.88, 0.94]) followed by mRNFL outer nasal

ring thickness (0.88 [0.86, 0.91]), GCC outer nasal ring thickness (0.87 [0.84, 0.89]) and GCIPL inner nasal ring thickness (0.79 [0.76, 0.82]).

Comparing *en-face* texture analysis results to instrument measured tissue thickness measurements for differentiating between glaucoma and healthy eyes, texture analysis significantly improved on 8 of 10 GCIPL total ring or within ring sector measurements (all comparisons $p \leq 0.03$), on 6 of 10 macular RNFL measurements (all comparisons $p \leq 0.004$) and on 2 GCC measurements (both comparisons $p \leq 0.03$) according to Wald bootstrap covariance testing. AUPRCs also are shown to compare relative differences in results when controlling for the glaucoma versus healthy sample size imbalance.

Figure 3 illustrates an example of thickness images from a healthy eye wrongly classified as glaucomatous by all tissue thickness measurements but correctly classified by *en-face* texture analysis. A classification cut-off of 0.50 was used. Subjective assessment of these images suggests symmetrical superior and inferior hemiretina tissue thickness with substantial thickness in both hemiretinae. Figure 4 illustrates an example of thickness images from a glaucomatous eye wrongly classified as healthy by GCIPL thickness but correctly classified as glaucoma by *en-face* texture analysis and all other thickness measurements. Subjective assessment of these images suggests decreased inferior *en-face* texture and tissue thinning of the inferior macular RNFL and GCC corresponding with a superior arcuate visual field defect. No glaucoma related defect is apparent in the GCIPL image.

Results for the best performing measurements for all tissue types and for *en-face* texture analysis (total inner ring thickness and total outer ring thickness) in highly myopic eyes (AL > 27 mm) are shown in Table 4. Results indicate that diagnostic accuracy for texture-based analysis was highest in the outer measurement ring (0.92 [0.89, 0.94]), accuracy for GCIPL thickness was highest in the inner measurement ring (0.86 [0.84, 0.88]), accuracy for mRNFL thickness was highest in the outer measurement ring (0.84 [0.81, 0.87]), and accuracy for GCC thickness was highest in the outer measurement ring (0.86 [0.84, 0.8]). The best texture-based AUROC was significantly higher than the best GCC thickness AUROC. In all cases, our novel texture analysis improved on tissue thickness measurements according to Wald bootstrap covariance testing in this AL > 27 mm subset analysis (all $p \leq 0.02$).

Similar results in age-matched and race-matched eyes are shown in Supplementary Tables 1 and 2.

Discussion

The current results suggest that our novel en-face texture-based analysis method can improve on most investigated tissue thickness measurements for discriminating between highly myopic glaucomatous and highly myopic healthy eyes. This likely is attributable in part to its reliance on minimal tissue segmentation (segmentation of the ILM only) because attempts at multi-layer segmentation tend to fail more frequently in highly myopic eyes. In

addition, the texture-based approach may be measuring neural tissue, while GCIPL, mRNFL and GCC thickness measurements include both neural and non-neural tissue.

We believe that the analysis of minimally segmented *en-face* images improves glaucoma versus healthy classification in highly myopic eyes, in part, because most software that incorporates segmentation of multiple tissue layers uses smoothing techniques that may mask small, local defects or changes in tissue thickness, while our methods does not use such techniques. For instance Lu et al.[20] employed smoothing by interpolation using a bilateral filter to retain the appearance of continuous segmented tissue after the removal of vessels in OCT images. It is possible that this smoothing technique could decrease the detection of focal defects located adjacent to vessels. Similarly Ehnes and colleagues[21] employed instrument software-independent cubic spline fitting across 30 image pixels in images obtained by the Zeiss Stratus, Optovue RTVue and Heidelberg Spectralis devices. Although the thickness of individual retinal layers did not deviate greatly across instruments and 30 images pixels is not a large contour from which to interpolate, it is still possible that small defects in tissue thickness remained undetected. It should be noted that the texture-based method described herein also theoretically is independent of the instrument software.

To determine if a longitudinal change in cpRNFL reflectance (a measure related to texture because both are a function of illumination) was predictive of the rate of change in functional measurements in glaucoma eyes, Gardiner and colleagues[22] compared the predictive power of the rate of cpRNFL thinning to the predictive power of the rate of reflectance intensity ratio for predicting the rate of the mean perimetric defect. For a given rate of cpRNFL thinning, a reduction in the cpRNFL reflectance intensity ratio was associated with a more rapid functional deterioration. These results suggest that incorporating OCT reflectance information may improve the structure–function relationship in glaucoma.

Finally and related, it is possible that *en-face* information can be combined with tissue thickness measurements to better identify RNFL abnormalities in glaucoma. Leung et al. reported that integrating wide-field OCT RNFL thickness measurement (including parapapillary and macula regions) with OCT-based RNFL reflectance data (called Retinal Nerve Fiber Layer Optical Texture Analysis, ROTA) resulted in a similar sensitivity with a specificity improved by almost 0.20 for classifying glaucomatous and healthy eyes compared to RNFL thickness measurements alone.[23] In addition, RNFL reflectance measurements were more strongly associated with the mean perimetric defect than RNFL with thickness measurements. While these results are promising for classifying glaucomatous and healthy eyes, it has not yet been determined if ROTA will succeed when applied to highly myopic glaucomatous eyes because OCT RNFL thickness measurements still require successful tissue segmentation that can be difficult in myopic eyes.

Recently, because of the complexities involved in diagnosing glaucoma in myopic eyes, the development of normative databases including myopic eyes for the diagnosis of glaucoma has been suggested. Evidence suggests that the use of such databases increases specificity for detecting glaucoma in myopic eyes without decreasing sensitivity.[24,25] Because the

method described herein is less susceptible to the effect of myopia on segmentation failure than tissue thickness measurements, we provide evidence that inclusion of texture, a novel parameter into normative myopia databases may improve our ability to differentiate between healthy and glaucoma eyes with high myopia.

The current study has several limitations. First, the cohort of highly myopic eyes is relatively small. A small sample size generally reduces the ability to detect significant differences, but also may be biased in some way and not represent the general population of eyes with axial high myopia. We did, however, find significantly better diagnostic accuracy for our *en-face* method even with the small sample. The disadvantage of a relatively small sample size may thus serve to strengthen the conclusion of the study. Second, there was a significant difference in age between the experimental groups, although this possible confound was controlled for in all analyses. For this reason, we performed subset analyses using age-matched (and race-matched) populations and showed similar results compared to those observed using unbalanced data sets (the diagnostic accuracy of the current texture-based analysis method was significantly better than most investigated tissue thickness measurements). Finally, using the currently described method, the segmentation of one layer (the ILM) is still required, but because of the difference in contrast between the ILM and the adjacent vitreous, this layer is usually easily segmented.

In conclusion, the texture-based *en-face* image analysis described herein shows improved discrimination between glaucoma and healthy axial highly myopic eyes. While further investigation is needed, the current methodology shows promise for improving the detection of glaucoma in eyes with high myopia where traditional retinal layer segmentation becomes more challenging.

Supplementary Material

Refer to Web version on PubMed Central for supplementary material.

Acknowledgements / Disclosures

Funding/Support:

National Institutes of Health/National Eye Institute, Bethesda MA: R01 EY029058, R21 EY027945, K99 EY030942 P30 EY022589, R01 EY027510.

An unrestricted grant from Research to Prevent Blindness, New York NY.

Participant retention incentive grants in the form of glaucoma medication at no cost from Novartis/Alcon Laboratories Inc, Allergan, Akorn and Pfizer Inc.

Financial Disclosures:

C. Bowd - None

A. Belghith – None

J. Rezapour - None

M. Christopher – None

L. Hyman – None

J.B. Jonas – None

R.N. Weinreb - Consultant: Aerie Pharmaceuticals, Allergan, Bausch & Lomb, Eyenovia, Implantdata, Novartis; Research Support: Bausch and Lomb, Carl Zeiss Meditec, Centervue, Heidelberg Engineering, Konan Medical, Optovue.

L.M. Zangwill - Research Support: Carl Zeiss Meditec, Heidelberg Engineering, Optovue, Topcon Medical Systems

References

1. Holden BA, Fricke TR, Wilson DA, et al. Global Prevalence of Myopia and High Myopia and Temporal Trends from 2000 through 2050. Ophthalmology. May 2016;123(5):1036–42. doi:10.1016/j.ophtha.2016.01.006 [PubMed: 26875007]
2. Ikuno Y. Overview of the Complications of High Myopia. Retina-J Ret Vit Dis. Dec 2017;37(12):2347–2351. doi:Doi 10.1097/Iae.0000000000001489
3. Marcus MW, de Vries MM, Montolio FGJ, Jansonius NM. Myopia as a Risk Factor for Open-Angle Glaucoma: A Systematic Review and Meta-Analysis. Ophthalmology. Oct 2011;118(10):1989–U146. doi:10.1016/j.ophtha.2011.03.012 [PubMed: 21684603]
4. Xu L, Wang Y, Wang S, Wang Y, Jonas JB. High myopia and glaucoma susceptibility the Beijing Eye Study. Ophthalmology. Feb 2007;114(2):216–20. doi:10.1016/j.ophtha.2006.06.050 [PubMed: 17123613]
5. Tan NYQ, Sng CCA, Ang M. Myopic optic disc changes and its role in glaucoma. Curr Opin Ophthalmol. Mar 2019;30(2):89–96. doi:10.1097/ICU.0000000000000548 [PubMed: 30562243]
6. Hwang YH, Yoo C, Kim YY. Myopic Optic Disc Tilt and the Characteristics of Peripapillary Retinal Nerve Fiber Layer Thickness Measured by Spectral-domain Optical Coherence Tomography. Journal of Glaucoma. Apr-May 2012;21(4):260–265. doi:10.1097/IJG.0b013e31820719e1 [PubMed: 21623226]
7. Leung CKS, Yu M, Weinreb RN, et al. Retinal Nerve Fiber Layer Imaging with Spectral-Domain Optical Coherence Tomography: Interpreting the RNFL Maps in Healthy Myopic Eyes. Invest Ophth Vis Sci. Oct 2012;53(11):7194–7200. doi:10.1167/iovs.12-9726
8. Tan NYQ, Sng CCA, Jonas JB, Wong TY, Jansonius NM, Ang M. Glaucoma in myopia: diagnostic dilemmas. Brit J Ophthalmol. Oct 2019;103(10):5–13. doi:10.1136/bjophthalmol-2018-313530
9. Ganekal S, Sadhwini MH, Kagathur S. Effect of myopia and optic disc area on ganglion cell-inner plexiform layer and retinal nerve fiber layer thickness. Indian J Ophthalmol. Jul 2021;69(7):1820–1824. doi:10.4103/ijo.IJO_2818_20 [PubMed: 34146037]
10. Kim YW, Lee J, Kim JS, Park KH. Diagnostic Accuracy of Wide-Field Map from Swept-Source Optical Coherence Tomography for Primary Open-Angle Glaucoma in Myopic Eyes. Am J Ophthalmol. Oct 2020;218:182–191. doi:10.1016/j.ajo.2020.05.032 [PubMed: 32574775]
11. Hood DC, Fortune B, Mavrommatis MA, et al. Details of Glaucomatous Damage Are Better Seen on OCT En Face Images Than on OCT Retinal Nerve Fiber Layer Thickness Maps. Invest Ophthalmol Vis Sci. Oct 2015;56(11):6208–16. doi:10.1167/iovs.15-17259 [PubMed: 26426403]
12. Hwang YH, Kim MK, Kim DW. Segmentation Errors in Macular Ganglion Cell Analysis as Determined by Optical Coherence Tomography. Ophthalmology. May 2016;123(5):950–958. doi:10.1016/j.ophtha.2015.12.032 [PubMed: 26854040]
13. Sample PA, Girkin CA, Zangwill LM, et al. The African Descent and Glaucoma Evaluation Study (ADAGES): design and baseline data. Arch Ophthalmol. Sep 2009;127(9):1136–45. doi:127/9/1136 [pii] 10.1001/archophthalmol.2009.187 [PubMed: 19752422]
14. Azad R, Asadi-Aghbolaghi M, Fathy M, Escalera S. Bi-Directional ConvLSTM U-Net with Densley Connected Convolutions. Ieee Int Conf Comp V. 2019:406–415. doi:10.1109/Iccvw.2019.00052
15. Jonas JB, Ohno-Matsui K, Panda-Jonas S. Optic Nerve Head Histopathology in High Axial Myopia. Journal of Glaucoma. Feb 2017;26(2):187–193. doi:10.1097/Ijg.0000000000000574 [PubMed: 27846047]
16. Rezapour J, Bowd C, Dohleman J, et al. The influence of axial myopia on optic disc characteristics of glaucoma eyes. Sci Rep-Uk. Apr 23 2021;11(1)doi:ARTN 8854 10.1038/s41598-021-88406-1

17. Margolin R, Zelnik-Manor L, Tal A. OTC: A Novel Local Descriptor for Scene Classification. Lect Notes Comput Sc.2014;8695:377–391.

18. Bang S, Edell E, Yu Q, Pratzer K, Stark W. Accuracy of intraocular lens calculations using the IOLMaster in eyes with long axial length and a comparison of various formulas. Ophthalmology. Mar 2011;118(3):503–6. doi:10.1016/j.ophtha.2010.07.008 [PubMed: 20884057]

19. El-Nafees R, Moawad A, Kishk H, Gaafar W. Intra-ocular lens power calculation in patients with high axial myopia before cataract surgery. Saudi J Ophthalmol. Jul 2010;24(3):77–80. doi:10.1016/j.sjopt.2010.03.006 [PubMed: 23960880]

20. Lu SJ, Cheung CYL, Liu JA, Lim JH, Leung CKS, Wong TY. Automated Layer Segmentation of Optical Coherence Tomography Images. Ieee T Bio-Med Eng. Oct 2010;57(10):2605–2608. doi:10.1109/Tbme.2010.2055057

21. Ehnes A, Wenner Y, Friedburg C, et al. Optical Coherence Tomography (OCT) Device Independent Intraretinal Layer Segmentation. Translational Vision Science & Technology. Jan 2014;3(1)doi:ARTN 1 10.1167/tvst.3.1.1

22. Gardiner SK, Demirel S, Reynaud J, Fortune B. Changes in Retinal Nerve Fiber Layer Reflectance Intensity as a Predictor of Functional Progression in Glaucoma. Invest Ophthalmol Vis Sci. Mar 2016;57(3):1221–7. doi:10.1167/iovs.15-18788 [PubMed: 26978028]

23. Leung CK. Retinal nerve fiber layer (RNFL) Optical Texture Analysis (ROTA) for evaluation of RNFL abnormalities in glaucoma. Invest Ophthalmol Vis Sci. 2018;59:3497. [PubMed: 30025073]

24. Biswas S, Lin C, Leung CK. Evaluation of a Myopic Normative Database for Analysis of Retinal Nerve Fiber Layer Thickness. JAMA Ophthalmol. Sep 1 2016;134(9):1032–9. doi:10.1001/jamaophthalmol.2016.2343 [PubMed: 27442185]

25. Nakanishi H, Akagi T, Hangai M, et al. Sensitivity and specificity for detecting early glaucoma in eyes with high myopia from normative database of macular ganglion cell complex thickness obtained from normal non-myopic or highly myopic Asian eyes. Graef Arch Clin Exp. Jul 2015;253(7):1143–1152. doi:10.1007/s00417-015-3026-y

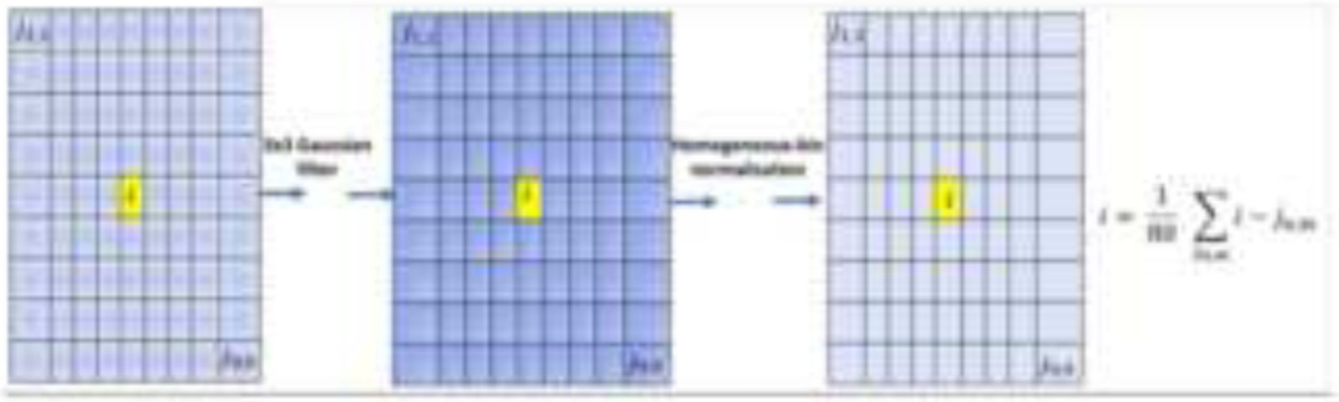

Figure 1:
Steps for the SALSA-Texture image transformations where i is a given image pixel and j_n, are the surrounding pixels.

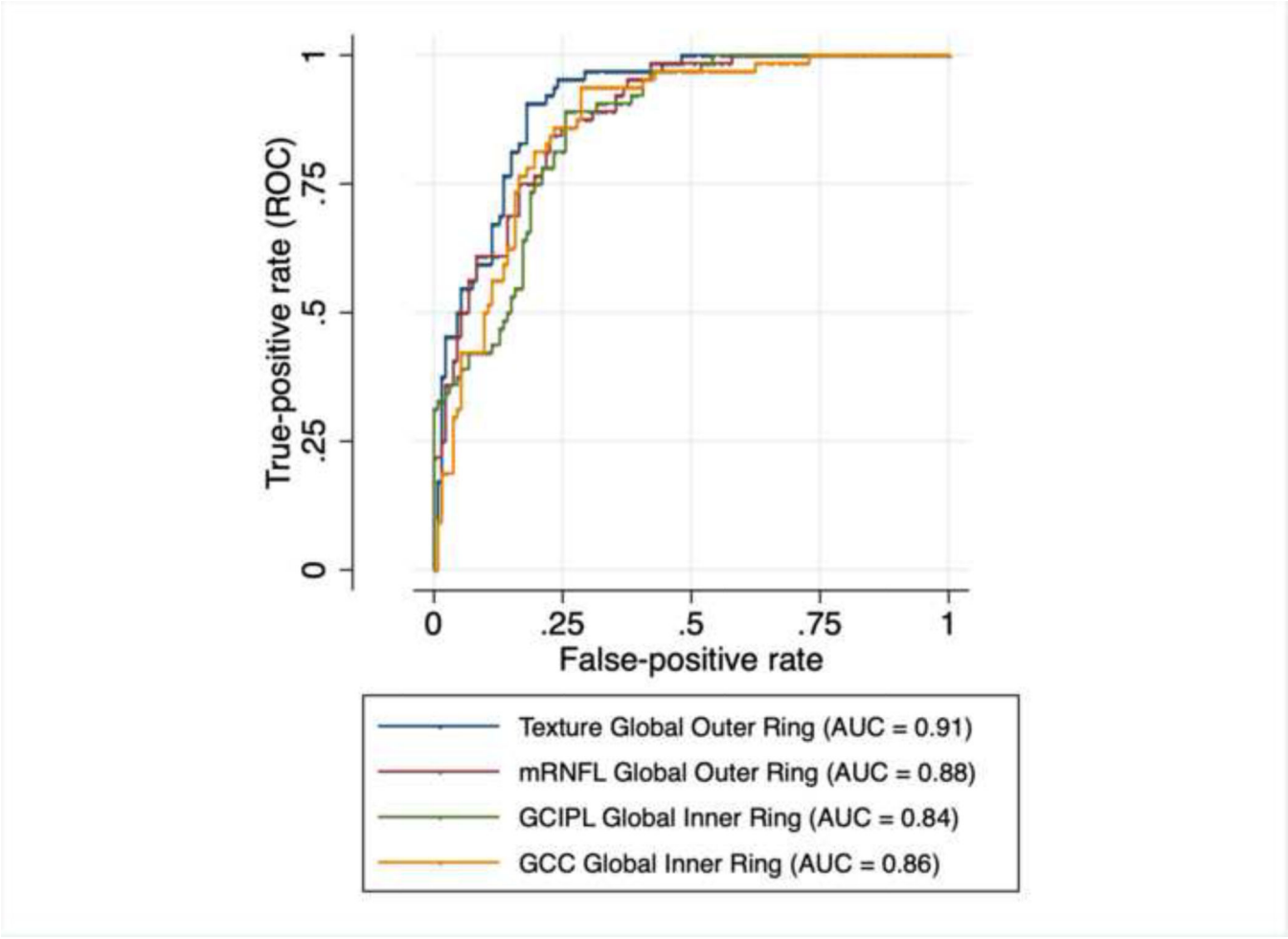

Figure 2:
AUROCs for the best texture-based, GCIPL thickness-based, mRNFL thickness-based, and GCC thickness-based regional measurements.

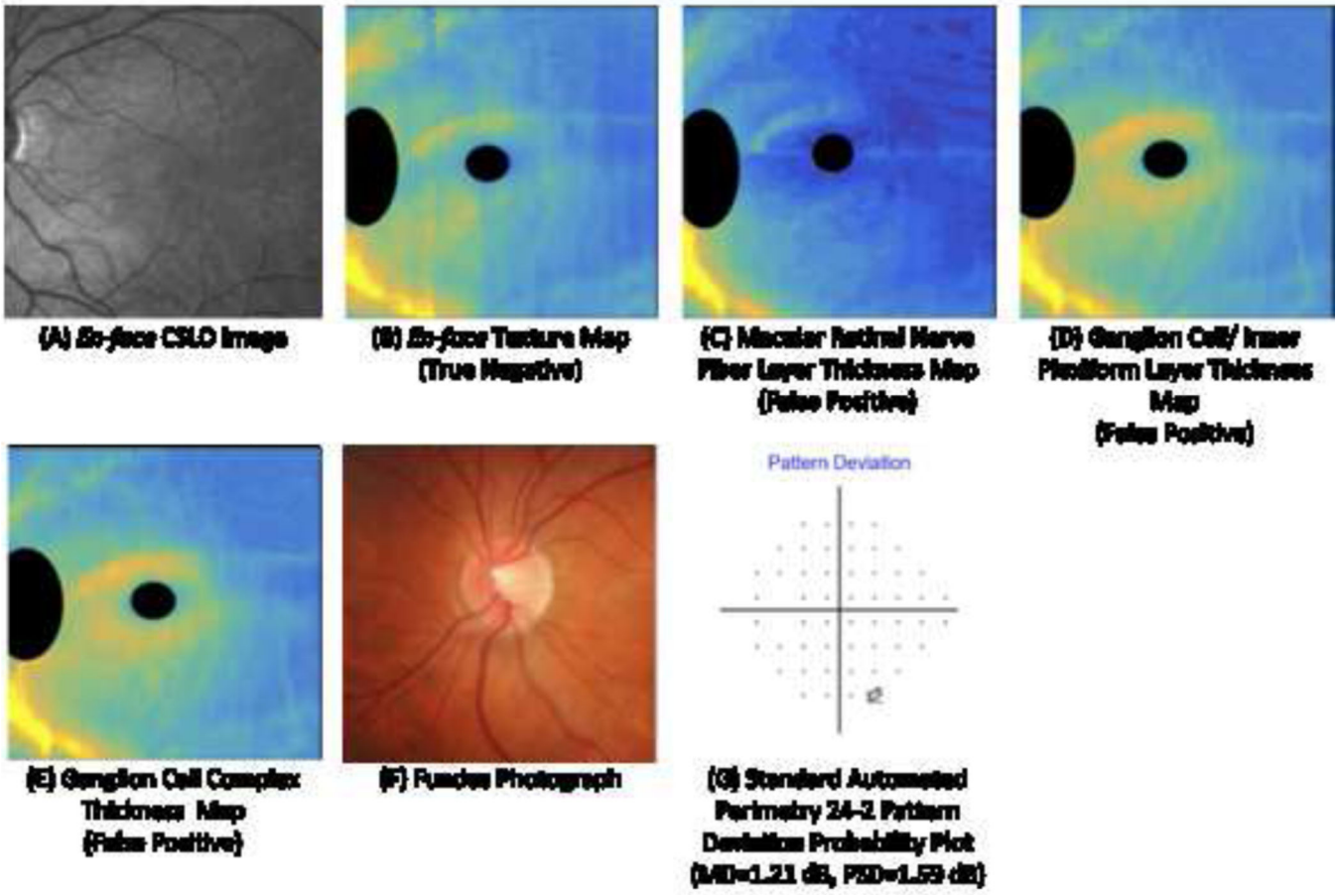

Figure 3:

Example a healthy eye correctly classified by (B) *En-face* Texture Map but incorrectly classified by (C) Macular Retinal Nerve Fiber Layer Thickness Map, (D) Ganglion Cell/ Inner Plexiform Layer Thickness Map, (E) Ganglion Cell Complex Thickness Map. Panel (A) shows the *En-face* CSLO image for orientation purposes. (F) Fundus photograph and (G) Visual Field Pattern Deviation Plot obtained within six months of Spectralis imaging.

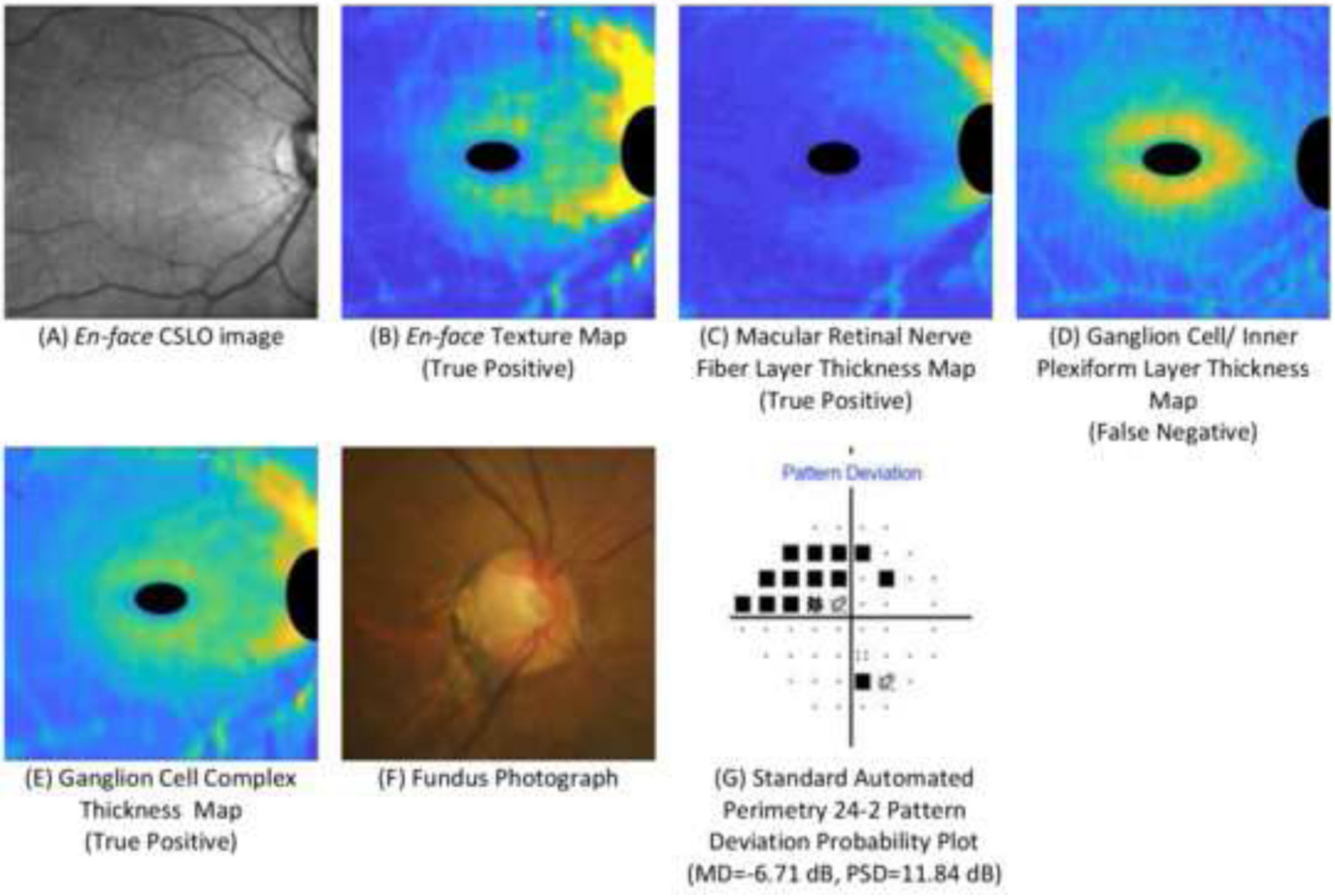

Figure 4:

Example a glaucomatous eye correctly classified by (B) *En-face* Texture Map, (C) Macular Retinal Nerve Fiber Layer Thickness Map and (E) Ganglion Cell Complex Thickness Map but incorrectly classified by (D) Ganglion Cell/ Inner Plexiform Thickness Map. Panel (A) shows the *En-face* CSLO image for orientation purposes. (F) Fundus photograph and (G) Visual Field Pattern Deviation Plot obtained within six months of Spectralis imaging.

Table 1:

Patient and eye characteristics by diagnosis. Mean values and 95% confidence intervals are shown for continuous variables. Statistical significance of differences in continuous and categorical variables are determined by two-sample t-tests and Fisher's exact test for patient level variables (respectively) and linear mixed effects models for eye level variables.

	Diagnosis		
	Healthy (n = 24, 44 Eyes)	**Glaucoma (n = 55, 92 Eyes)**	**p-value**
Age (years)	48.9 (46.7, 54.3)	65.9 (63.2, 68.5)	<0.001
Sex (% Female)	54.1%	43.6%	0.01
Race (%)			
Non-White	67.0%	42.0%	0.003
White	33.0%	58.0%	
MD (dB)	−1.42 (−1.89, 0.54)	−5.66 (−6.18, −4.17)	<0.001
IOP (mmHg)	15.39 (13.8, 16.1)	14.8 (14.1, 15.3)	0.52
AL (mm)	27.0 (26.2, 27.3)	27.1 (26.5, 27.3)	0.41
Spherical equivalent (D)	−7.35 (−7.67, −6.98)	−4.76 (−5.21, −4.31)	0.02
History of Cataract Surgery	13.69%	42.4%	<0.001

MD = Mean Deviation, IOP = Intraocular Pressure, AL = Axial Length

Table 2:

Measurements, estimated areas under the receiver operating characteristic curve (AUROC) and estimated areas under the precision recall curves (AUPRC) and for global measurements. (44 healthy eyes from 24 subjects and 92 glaucoma eyes from 55 patients).

			Univariable Analysis			
	Healthy	**Glaucoma**	**AUROC**	**(p-value) compared to texture**	**AUPRC**	**(p-value) compared to texture**
Texture (normalized image intensity)						
Global Inner ring	5.0 (4.9, 5.)	4.07 (3.9, 4.1)	0.90 (0.87, 0.92)		0.66 (0.62, 0.69)	
Global Outer ring	4.0 (3.9, 4.1)	3.21 (3.1, 3.3)	0.91 (0.88, 0.93)		0.68 (0.66, 0.71)	
GCIPL Thickness (μm)						
Global Inner ring	59.7 (58.0, 61.2)	49.0 (47.1, 50.9)	0.84 (0.82, 0.87)	0.07	0.59 (0.57, 0.62)	0.08
Global Outer ring	32.9 (32.0, 33.7)	30.6 (29.6, 31.7)	0.67 (0.61, 0.69)	0.001	0.61 (0.60, 0.63)	<0.001
mRNFL Thickness (μm)						
Global Inner ring	32.2 (30.3, 34.1)	24.7 (23.3, 26.1)	0.80 (0.78, 0.82)	0.004	0.55 (0.52, 0.58)	0.002
Global Outer ring	38.2 (36.2 40.2)	26.7 (25.1, 28.3)	0.88 (0.86, 0.91)	0.14	0.57 (0.53, 0.59)	<0.001
GCC Thickness (μm)						
Global Inner ring	96.1 (93.5 98.6)	77.4 (74.1, 80.6)	0.86 (0.84, 0.87)	0.03	0.57 (0.53, 0.59)	0.01
Global Outer ring	75.1 (73.0, 77.3)	61.1 (58.8, 63.48)	0.84 (0.82, 0.86)	<0.001	0.53 (0.51, 0.55)	<0.001

GCIPL = Ganglion Cell Inner-Plexiform Layer, mRNFL = macular Retinal Nerve Fiber Layer, GCC = Ganglion Cell Complex

Table 3:

Measurements, estimated areas under the receiver operating characteristic curve (AUROC) and estimated areas under the precision recall curves (AUPRC) and for sectoral measurements (44 healthy eyes from 24 subjects and 92 glaucoma eyes from 55 patients).

			Univariable Analysis			
	Healthy	**Glaucoma**	**AUROC**	**(p-value) compared to texture**	**AUPRC**	**(p-value) compared to texture**
Texture (normalized image intensity)						
Inner temporal	4.6 (4.5, 4.7)	3.8 (3.7, 4.0)	0.85 (0.82, 0.88)		0.61 (0.59, 0.62)	
Inner superior	4.8 (4.7, 5.0)	3.8 (3.6, 4.0)	0.84 (0.82, 0.87)		0.60 (0.58, 0.63)	
Inner nasal	5.6 (5.5, 5.8)	4.7 (4.5, 4.9)	0.87 (0.83, 0.89)		0.64 (0.61, 0.68)	
Inner inferior	4.9 (4.8, 5.1)	4.1 (3.9, 4.3)	0.86 (0.82, 0.88)		0.62 (0.60, 0.65)	
Outer temporal	3.1 (3.0, 3.2)	2.6 (2.6, 2.7)	0.88 (0.84, 0.89)		0.63 (0.61, 0.66)	
Outer superior	4.3 (3.9, 4.6)	3.1 (2.9, 3.1)	0.82 (0.80, 0.86)		0.60 (0.59, 0.63)	
Outer nasal	6.0 (5.8, 6.19)	4.6 (4.3, 4.8)	0.92 (0.88, 0.94)		0.69 (0.67, 0.73)	
Outer inferior	4.1 (4.0, 4.36)	3.1 (2.1, 3.1)	0.86 (0.82, 0.89)		0.61 (0.57, 0.63)	
GCIPL Thickness (μm)						
Inner temporal	67.5 (65.1, 69.8)	53.7 (51.2, 56.1)	0.83 (0.81, 0.85)	0.14	0.57 (0.54, 0.61)	0.34
Inner superior	44.1 (42.4, 45.8)	40.2 (38.7, 41.8)	0.75 (0.72, 0.80)	0.009	0.62 (0.57, 0.65)	0.46
Inner nasal	74.5 (71.8, 77.3)	60.6 (57.2, 63.9)	0.79 (0.76, 0.82)	0.03	0.56 (0.52, 0.59)	0.001
Inner inferior	50.3 (48.4, 52.1)	42.8 (41.0, 44.6)	0.77 (0.74, 0.81)	0.002	0.57 (0.53, 0.59)	0.003
Outer temporal	37.0 (35.9, 38.1)	32.2 (31.0, 33.4)	0.79 (0.76, 0.81)	<0.001	0.55 (0.53, 0.58)	<0.001
Outer superior	31.9 (29.8, 35.1)	27.1 (25.7, 28.6)	0.61 (0.58, 0.63)	<0.001	0.59 (0.57, 0.63)	0.45
Outer nasal	36.4 (31.2, 38.6)	30.0 (28.2, 31.8)	0.64 (0.61, 0.68)	<0.001	0.59 (0.58, 0.62)	<0.001
Outer inferior	32.2 (28.6, 35.8	30.0 (27.6, 31.4)	0.65 (0.61, 0.69)	<0.001	0.61 (0.59, 0.64)	0.03
mRNFL Thickness (μm)						
Inner temporal	21.1 (20.1, 22.1)	19.0 (18.2, 19.8)	0.67 (0.63, 0.69)	0.001	0.61 (0.60, 0.63)	0.19
Inner superior	40.0 (37.9, 42.2)	28.5 (26.0, 31.0)	0.8 (0.77, 0.83)	0.08	0.56 (0.53, 0.59)	0.36
Inner nasal	34.8 (31.2, 38.3)	27.1 (25.0, 29.1)	0.74 (0.72, 0.77)	<0.001	0.59 (0.57, 0.62)	0.07
Inner inferior	37.7 (35.4, 40.1)	29.6 (27.6, 31.6)	0.75 (0.73, 0.79)	<0.001	0.58 (0.55, 0.64)	0.17
Outer temporal	20.4 (19.7, 21.2)	18.4 (17.8, 19.0)	0.69 (0.67, 0.73)	<0.001	0.61 (0.60, 0.63)	0.22
Outer superior	47.6 (43.7, 51.4)	32.0 (29.1, 34.9)	0.83 (0.78, 0.85)	0.11	0.58 (0.54, 0.61)	0.65
Outer nasal	80.7 (77.4, 83.9)	53.1 (49.0, 57.3)	0.87 (0.85, 0.91)	0.21	0.59 (0.57, 0.63)	<0.001
Outer inferior	45.1 (42.4, 47.9)	30.6 (28.0, 33.1)	0.82 (0.80, 0.84)	0.29	0.54 (0.51, 0.58)	0.12
GCC Thickness (μm)						
Inner temporal	89.2 (86.9, 91.5)	73.2 (70.3, 76.0)	0.84 (0.81, 0.87)	0.54	0.55 (0.50, 0.57)	0.001
Inner superior	90.9 (87.9, 93.8)	71.5 (68.0, 75.1)	0.82 (0.80, 0.85)	0.34	0.54 (0.52, 0.58)	0.09
Inner nasal	111.2 (107.9, 114.5)	90.6 (86.4, 94.8)	0.81 (0.79, 0.84)	0.08	0.53 (0.50, 0.55)	0.002
Inner inferior	92.3 (89.1, 95.6)	77.2 (72.4, 82.1)	0.79 (0.77, 0.83)	0.09	0.50 (0.48, 0.53)	0.001

			Univariable Analysis			
	Healthy	**Glaucoma**	**AUROC**	**(p-value) compared to texture**	**AUPRC**	**(p-value) compared to texture**
Outer temporal	58.4 (56.9, 59.9)	50.4 (48.9, 52.0)	0.81 (0.78, 0.84)	0.08	0.53 (0.51, 0.56)	<0.001
Outer superior	80.8 (72.9, 88.7)	67.2 (57.1, 77.4)	0.81 (0.78, 0.84)	0.43	0.55 (0.52, 0.57)	0.03
Outer nasal	114.5 (110.9, 118.1)	86.81 (82.5, 91.1)	0.87 (0.84, 0.89)	0.09	0.52 (0.50, 0.55)	<0.001
Outer inferior	79.3 (73.5, 85.0)	73.34 (56.8, 76.9)	0.81 (0.79, 0.83)	0.08	0.56 (0.53, 0.58)	0.08

GCIPL = Ganglion Cell Inner-Plexiform Layer, mRNFL = macular Retinal Nerve Fiber Layer, GCC = Ganglion Cell Complex

Table 4:

Measurements, estimated areas under the receiver operating characteristic curve (AUROC) and estimated areas under the precision recall curves (AUPRC) and for high myopic eyes (axial length >27 mm) (22 healthy eyes from 12 subjects and 38 glaucoma eyes from 24 patients).

			Univariable			
	Healthy	**Glaucoma**	**AUROC**	**(p-value) compared to texture**	**AUPRC**	**(p-value) compared to texture**
Texture (normalized image intensity)						
Global Inner ring	5.0 (4.8, 5.2)	3.4 (3.2, 3.7)	0.91 (0.89, 0.93)		0.67 (0.65, 0.71)	
Gloabl Outer ring	3.9 (3.7, 4.2)	2.7 (2.4, 2.9)	0.92 (0.89, 0.94)		0.69 (0.67, 0.73)	
GCIPL Thickness (μm)						
Global Inner ring	58.8 (56.0, 61.6)	45.5 (42.3, 48.7)	0.86 (0.84, 0.88)	0.02	0.61 (0.58, 0.63)	0.002
Global Outer ring	32.2 (31.0, 33.5)	29.2 (27.6, 30.7)	0.68 (0.63, 0.72)	0.001	0.57 (0.55, 0.59)	<0.001
mRNFL Thickness (μm)						
Global Inner ring	32.9 (30.0, 35.8)	24.7 (22.0, 27.5)	0.80 (0.77, 0.81)	<0.001	0.54 (0.50, 0.56)	0.001
Global Outer ring	36.2 (33.4, 39.1)	25.9 (23.4, 28.4)	0.84 (0.81, 0.87)	<0.001	0.53 (0.51, 0.56)	<0.001
GCC Thickness (μm)						
Global Inner ring	96.1 (91.8, 100.4)	73.8 (67.5, 80.0)	0.85 (0.82, 0.87)	0.003	0.55 (0.51, 0.57)	0.004
Global Outer ring	73.8 (70.4, 77.2)	58.2 (54.3, 62.01)	0.86 (0.84, 0.88)	0.002	0.53 (0.51, 0.55)	<0.001

GCIPL = Ganglion Cell Inner-Plexiform Layer, mRNFL = macular Retinal Nerve Fiber Layer, GCC = Ganglion Cell Complex